ONLINE INFORMATION

Reagents

The anti-human cystic fibrosis transmembrane conductance regulator (CFTR) antibody used to detect CFTR in baby hamster kidney fibroblast cells ("antibody 596") the CFTR corrector therapeutic "C18" (CF-106951; Vertex patent WO 2007/021982A2; 1-(benzo[d][1,3]dioxol-5-yl)-N-(5-((2-chlorophenyl)(3-hydroxypyrrolidin-1-yl)methyl)thiazol-2-yl)cyclopropanecarboxamide) were acquired through the *Cystic Fibrosis Foundation Therapeutics* Chemical and Antibody Distribution Programs (http://www.cff.org/research). Dr. John Riordan (University of North Carolina - Chapel Hill) provided the "596 CFTR antibody" and Dr. Robert Bridges (Rosalind Franklin University of Medicine and Science, Chicago, USA) provided the C18 compound. The 596 CFTR antibody targets amino acids 1204-1211 (i.e., located in nucleotide binding domain 2) (1).

Fluorescein-labeled S1P (FITC-S1P) was purchased from Echelon Biosciences (via Cedarlane Laboratories; Burlington, Canada); lumacaftor was purchased from Selleck Chemicals (Cedarlane Laboratories); recombinant tumor necrosis factor was purchased from Sigma-Aldrich Canada (Oakville, Canada; cat# T6674); and protease inhibitor cocktail tablets (Complete®; used in western blot lysis buffers) were purchased from Roche (Mississauga, Canada). All other chemical reagents were purchased from Sigma-Aldrich. MOPS-buffered salt solution contained [mmol/L]: NaCl 145, KCl 4.7, $CaCl_2$ 3.0, $MgSO_4$ •$7H_2O$ 1.17, NaH_2PO_4 •$2H_2O$ 1.2, pyruvate 2.0, ethylenediaminetetraacetic acid (EDTA) 0.02, 3-morpholinopropanesulfonic acid (MOPS) 3.0, and glucose 5.0.

CFTR Mutant and Knockout Mice

Male mice homozygous for the ΔF508 CFTR mutation ($CFTR^{tm1EUR}$; designated "ΔF508" in the present study) (2), CFTR gene deletion ($CFTR^{tm1Unc}$; designated $CFTR^{-/-}$) and the complimentary wild-type control littermates were obtained from an established colony at the *Hospital for Sick Children*, Toronto (all $CFTR^{-/-}$, $CFTR^{\Delta F508}$ and wild-type littermates are mixed strains).

In our hands, we found that $CFTR^{-/-}$ mice were highly prone to dying under anesthesia. While this mortality was not an issue for experiments involving cerebral artery isolation (e.g., Figures 3C and 5C), it significantly confounded cerebral blood flow and systemic hemodynamic measurements. Unlike $CFTR^{-/-}$ mice, $CFTR^{\Delta F508}$ mutant mice were not nearly as prone to dying during anesthesia. Since the $CFTR^{\Delta F508}$ mutation profoundly reduces CFTR trafficking to the plasma membrane (3), CFTR activity is very low in the $CFTR^{\Delta F508}$ mouse model (2,4,5). Thus, the $CFTR^{\Delta F508}$ model provided an adequate alternative to $CFTR^{-/-}$mice for cerebral blood flow and systemic hemodynamic measurements. We did not pursue the underlying cause of the $CFTR^{-/-}$ mortality.

Both $CFTR^{-/-}$ and $CFTR^{\Delta F508}$ are widely known to adversely react to stress. As examples, housing conditions and transport are two notable stressors that can significantly increase mortality (6). Interestingly, $CFTR^{\Delta F508}$ mice display a less severe phenotype than $CFTR^{-/-}$ mice (5,6): this is presumed to be due to the small amount of residual CFTR activity that is present in $CFTR^{\Delta F508}$ animals (2). In this context, we suspect that the $CFTR^{-/-}$ mice may have been more sensitive to external environmental stressors in our animal facility (e.g., housing conditions, noise and handling), which ultimately manifested in heightened mortality under anesthesia.

As an experimental model, $CFTR^{\Delta F508}$ mice possess several abnormalities associated with the loss of CFTR function. Intestinal complications are the most pronounced pathological effect of the CFTR mutation: this also represents the primary cause of post-natal mortality (6,7). Common gastrointestinal issues include thick mucus retention, dysmotility and a strong propensity for bowel obstruction. $CFTR^{\Delta F508}$ mice are 40-50% smaller in weight/size relative to wild-type counterparts, although they thrive well into adulthood (6,7). Several other differences relative to wild-type mice have been

observed; however, these appear to be relatively minor (6,7). For example, altered chloride currents and/or sodium transport have been noted in certain tissues (e.g., kidney, gall bladder, nasal epithelium), but the pathological significance of these differences is not clear, since the tissues do not appear to be histologically compromised (6,7).

Of note, $CFTR^{\Delta F508}$ mice (and CFTR mutant mice in general) possess a rather mild cystic fibrosis phenotype in relation to human cystic fibrosis. The lower respiratory tract of $CFTR^{\Delta F508}$ mice is essentially normal: there are no lower airway epithelial abnormalities and lung inflammation does not spontaneously develop without challenge (6,7). The pancreas, gall bladder, liver, bile duct, male reproductive tract, lacrimal gland and submandibular glands display no obvious histopathology (5-7). The lack of a severe cystic fibrosis phenotype is partially attributed to the expression of a non-CFTR, calcium-activated chloride channel (CACC) in certain mouse tissues that compensates for the loss of CFTR (7,8).

Global hemodynamic parameters

As previously described (9-11), echocardiographic measurements were collected with a 30 MHz mechanical sector transducer (Vevo 770; Visual Sonics, Toronto, Canada) in conjunction with the mean arterial pressure (MAP) measurements (Millar SPR-671 micro-tip mouse pressure catheter; Inter V Medical Inc., Montreal, Canada). The aortic flow velocity-time integral (VTI) was measured using pulse wave Doppler just above the aortic root. The aortic cross-sectional area (CSA) was calculated from the aortic root dimension (ARD): $CSA = \pi(ARD/2)^2$. Stroke volume (SV), CO and TPR were calculated as: SV = CSA x VTI; CO = SV x HR; TPR = MAP/CO.

MRI-based measurement of cerebral perfusion

As described in our previous investigations (10-12), we utilized a flow-sensitive alternating inversion recovery (FAIR) magnetic resonance imaging (MRI) technique (13) to evaluate cerebral blood flow (CBF).

During imaging, mice were immobilized with 1.8% isoflurane delivered through a nose cone. To maintain body temperature, the MRI is equipped with embedded tubes that convect water from an external heater-pump. Respiration was monitored using a pneumatic pillow (SA Instruments, Stonybrook, USA); isoflurane levels were adjusted to maintain respiration at approximately 50 breaths/minute.

FAIR images were obtained using a 7 Tesla micro-MRI system (BioSpec 70/30 USR, Bruker BioSpin, Ettlingen, Germany), including the B-GA12 gradient insert, 72 mm inner diameter linear volume resonator for RF transmission, and anteriorly placed head coil for RF reception. FAIR isolates perfusion as an accelerated T_1 signal relaxation following slice-selective compared to non-selective inversion preparation, as per the following equation: $CBF = \lambda\ (1/T_{1,ss} - 1/T_{1,ns})$ (ml/(100g*min), where '**ss**' and '**ns**' denote slice-selective and non-selective measurements and λ is the blood-brain partition coefficient, defined as the ratio between water concentration per g brain tissue and per ml blood. This coefficient is approximately 90 ml/100g in mice (14).

The FAIR optimization used in our study was a single-shot echo planar imaging (EPI) technique with preceding adiabatic inversion. Parameters included echo time of 12.5 ms, repetition time of 17 s, 18 inversion times ranging from 25-to-6825 ms in 400 ms increments, 3 mm slice-selective inversion slab, 18x18 mm field-of-view with 72x72 matrix for 250 μm in-plane resolution, 1 mm slice thickness, and 10 min 12 s data acquisition time. Acquisitions were repeated in fore-, mid-, and hind-brain vertical sections, corresponding to anterior, mixed, and posterior circulations.

FAIR images were evaluated by manual prescription (MIPAV, NIH, Bethesda, MD; http://mipav.cit.nih.gov) of sub-hemispheric regions-of-interest (ROIs), termed 'global', and local ROIs corresponding to cortical and sub-cortical parenchyma in forebrain sections; cortical and paraventricular parenchyma in middle sections; and cortical and midbrain parenchyma in hindbrain sections. ROIs were drawn directly on T_1-weighted signal images to enable manual correction for intra-scan motion. ROIs were registered with parametric CBF maps to verify absence of bias from high perfusion vessels and meninges. T_1 regressions and CBF calculations were performed using Matlab (Mathworks, Natick, MA). All reported CBF values fall within the published range of murine CBF measures for the isoflurane level utilized in this study (15).

EPI is particularly prone to magnetic susceptibility-related distortion in the phase-encoding direction (16), which corresponds to the vertical direction in this FAIR protocol. As evidenced in Online Figure 1, shimming did not sufficiently constrain EPI distortion in the subarachnoid hemorrhage (SAH) surgical model, due to air-tissue boundaries immediately adjacent to the brain at the imaging time-points post-surgery. In certain cases, the distortion was severe enough that the ROIs needed to be placed more laterally in the cortex (Online Figure 1). However, because the distortion is consistent in all T_1-weighted images, this does not bias the T_1 measurement, provided the distorted region does not overlap with another region. The relatively consistent ns-T_1 values within each cohort (i.e., 7% standard deviation between cohorts, no treatment group differences within cohorts) provide supporting evidence that distortion bias had a negligible impact on the CBF measurements.

Cell Culture

We have previously described the procedures for isolating and culturing mesenteric artery smooth muscle cells (10). Briefly, mesenteric artery segments were isolated, cut into small pieces and digested with trypsin, collagenase and elastase. The resulting cell suspension was washed several times in phosphate-buffered saline and plated in Dulbecco's Modified Eagle Medium (DMEM) culture media containing 10% fetal bovine serum and 1% penicillin-streptomycin. Cell cultures were maintained at 37°C with 5% CO_2 and split at 10^6 cells seeding density.

Baby hamster kidney fibroblast cells stably expressing wild-type human CFTR (10,17) were maintained in DMEM/F12 media containing 5% fetal bovine serum and 250 μmol/L methotrexate (which activates the CFTR transgene promoter). Cells were maintained under standard cell culture conditions at 37°C with 5% CO_2.

FACS-based measurement of FITC-S1P uptake

As previously described (10), cell monolayers (treated or untreated) were incubated with 1 μmol/L S1P-FITC for 60 minutes; the cells were then detached by trypsinization, washed twice with ice-cold PBS, filtered through a 35 μm cell strainer and analyzed using the Becton-Dickinson FACS Canto operated by FACS DIVA version 6.1 software. Cell monolayers treated with non-labeled S1P served as background controls. The analysis procedure determined the mean fluorescence intensity (arbitrary units) of each cell population, which is a measure of uptake.

Iodide Efflux Assessments

Iodide efflux measurements were conducted as previously described (18). Briefly, confluent cell monolayers were loaded with iodide by incubating them in a HEPES-based loading buffer (136 mmol/L NaI, 3 mmol/L KNO_3, 2 mmol/L $Ca(NO_3)_2$, 11 mmol/L glucose and 20 mmol/L HEPES; pH 7.4) for 1 hour (under standard cell culture conditions of 37°C in 5% CO_2). Following iodide loading, cells were washed 4x with iodide-free efflux buffer (where $NaNO_3$ is substituted for NaI).

Supernatant iodide levels were quantified with an iodide-selective electrode (Lazar Research Laboratories; Los Angeles, USA), calibrated with NaI standards. Pre-stimulation iodide levels were determined and then cells were stimulated with a cocktail containing 10 µmol/L forskolin, 1 mmol/L isobutylmethylxanthine and 100 µmol/L cpt-cAMP (in 1% v/v DMSO). The stimulation cocktail strongly activates PKA and consequently, maximally phosphorylates/activates CFTR. Supernatant iodide levels were determined over seven consecutive 1-minute intervals post-stimulation. Consistent with previous results (18), efflux was evident within the first minute and was reliably maximal between 60-120 seconds. The maximum efflux rate, therefore, was calculated using the measured efflux level between 60-120 seconds post-stimulation (18).

Western Blotting

Western blots for CFTR were completed as previously described (12,18). Cerebral artery lysates were prepared by grinding artery samples in lysis buffer containing 50 mM Tris (pH 7.3), 150 mM NaCl, 2 mM ETDA, 0.1% Triton-X-100, 0.1% SDS and protease inhibitors; the same lysis buffer was used to prepare cell culture lysates. Following lysis, the samples were centrifuged (10 minutes at 13,500 g; at 4^{o}C) to remove insoluble material. Immediately prior to polyacrylamide electrophoresis, additional SDS (to 2% final concentration), glycerol (to 2% final concentration), β-mercaptoethanol (to 2% final concentration) and dithiothreitol (2 mM final concentration) were added.

Proteins were separated electrophoretically on 7% acrylamide gels and transferred onto polyvinylidene difluoride (PVDF) membranes. The membranes were blocked for 30-40 minutes in 5% non-fat skim milk (in phosphate-buffered saline containing 1% Tween 20 (PBST); 137 mM NaCl, 2.7 mM KCl, 10 mM Na_2HPO_4, 1.76 mM K_2HPO_4; pH 7.4). Primary antibody treatments included:

(i) Rabbit polyclonal anti-CFTR (1:1,000 in 5% milk/PBST; *Cell Signaling Technology* via *New England Biolabs Canada*; Whitby, Canada; cat# 2269); cerebral artery and vascular smooth muscle cell lysates.
(ii) Mouse monoclonal anti-human CFTR (1:20,000 dilution in 5% milk/PBST; "antibody 596"); baby hamster kidney fibroblast cell lysates.
(iii) Mouse monoclonal anti-α-tubulin (1:5,000 in 5% milk/PBST; clone DM1A; *Cell Signaling Technology* via *New England Biolabs Canada*; cat# 3873).

The primary antibodies were conjugated with either peroxidase-labeled donkey anti-rabbit IgG (*GE Healthcare Amersham* (Piscataway, USA) cat# NA934) or peroxidase-labeled goat anti-mouse IgG (*GE Healthcare Amersham* cat# NA931) secondary antibodies. A standard chemiluminescence procedure (Westar ETA C; VPQ Scientific, Toronto, Canada) was used to expose X-ray film or collect digital images (ChemiDoc; Bio-Rad Laboratories; Mississauga, Canada). Developed films were evaluated densitometrically using "Image J" software (freely available from the NIH); digital images were evaluated with Image Lab software (Bio-Rad).

RNA Isolation and Reverse Transcription

Resistance artery RNA was isolated with *Norgen Biotek* (Thorold, Canada) "Total RNA Purification Micro" spin columns, using the proteinase K digestion and DNA removal procedures, as directed by the manufacturer's instructions. The eluted RNA was quantified with an *Agilent Technologies* RNA 6000 Pico Kit and Bioanalyzer; the analysis confirmed that high-quality RNA was retrieved from the artery tissue samples (RNA Integrity [RIN]: Cerebral=8.4±0.1, n=5; Cremaster=8.2±0.4, n=6). Isolation of RNA from Baby Hamster Kidney fibroblast cells followed the same procedure, with the omission of the proteinase K digestion step. In all cases, RNA was converted to cDNA using a "Superscript III" reverse transcription kit (*Invitrogen Life Technologies*; Burlington, Canada), according to the manufacturer's directions. Residual RNA was removed by incubating the resulting cDNA with RNAse H (0.125 U/µl; *New England Biolabs Canada*; Whitby, Canada).

Quantitative PCR

Quantitative PCR was performed using an *Applied Biosystems* ViiA ™ 7 Real Time PCR system and Power SYBR® Green PCR master mix (both distributed by *Invitrogen Life Technologies*). Each primer set (400 nmol/L in each reaction; Online Table 4) was rigorously validated to ensure specificity and comparable efficiency. Gene targets were assessed in triplicate, using 1 ng of cDNA generated from the reverse transcription; negative controls received water. The PCR amplification consisted of 10 minutes denaturation at 95°C, followed by 40 cycles of amplification (15 s at 95°C + 60 s at 60°C). Following amplification, the amplicons were melted: the resulting dissociation curve confirmed the production of single product. Transcript expression levels in mouse tissues were calculated from the ΔCt values relative to the standard housekeeping gene hydroxymethylbilane synthase (HMBS). To confirm that HMBS was reliable for normalization, transcript expression levels were also calculated from the ΔCt values relative to glucose-6-phosphate dehydrogenase (G6PD), which returned similar results. Experiments involving baby hamster kidney fibroblast cells used primers specific for human CFTR and hamster GAPDH, the latter serving as the housekeeping normalization gene.

Brain Fixation and Slide Preparation for Immunohistochemistry and Fluoro-Jade staining

The development of delayed vasoconstriction and brain injury is more rapid in the experimental mouse SAH model (2-5 days post-SAH) (12,19-21), compared to what is observed clinically (4-12 days post-SAH) (22,23). We selected the 2-days post-SAH induction time point for our injury marker assessments based on our previous work demonstrating significant neuronal injury and behavioral deficits at this time point (12).

At 2 days post-SAH induction, animals were anesthetized with isoflurane; their brains were perfused with phosphate buffered saline (PBS) and then perfusion fixed with phosphate-buffered paraformaldehyde (4%; pH 7.4), both via the ascending aorta. Brains were immediately dissected and cut into coronal sections 1mm posterior to the bregma. These brain sections were post-fixed in 4% paraformaldehyde (pH 7.4) for 48 hours at 4°C and then incubated in 10% sucrose (3 hours), followed by 30% sucrose overnight (at 4°C) for cyroprotection. The brain sections were then embedded in OCT (Sakura Finetek USA; Torrance, USA) on isopentane and dry ice. Cryostat sections (5µm thick coronal slices) were collected on "Tissue Path Superfrost Plus Gold" slides (Fisher Scientific; Whitby, Canada) and stored at -80°C until used.

Fluorescent Immunohistochemistry

All samples were pre-treated with 10-minute proteinase (20µg/ml; Promega; Madison, USA), followed by a standard 60-minute blocking procedure with either 10% normal donkey serum (Jackson ImmunoResearch Laboratories; West Grove, USA) in PBS or 10% goat serum (Invitrogen Life Technologies; Burlington, Canada) in PBS containing 1% bovine serum albumin. Brain slices were incubated with monoclonal rabbit anti-human active cleaved caspase-3 (clone C92-605; 1:1000 dilution; BD Biosciences Canada; Mississauga Canada) and conjugated with Alexa Fluor 488 goat anti-rabbit IgG (Invitrogen). Both antibodies were diluted in Can Get Signal® immunoreaction enhancer solution and used an incubation time of 1 hour at room temperature. Specimens were washed and mounted with CC Mount™.

Fluoro-Jade staining

Brain slices were serially incubated with 1% NaOH / 80% ethanol (5 minutes), 70% ethanol (2 minutes), distilled water (2 minutes) and 0.06% potassium permanganate (10 minutes). After washing with deionized water, brain slices were stained with 0.0004% Fluoro-jade B (Histo-Chem Inc., Jefferson, USA) in 0.1% acetic acid (15 minutes). The samples were then washed with deionized water, dried and cleared by immersion in xylene for 1 minute. Slides were mounted using DPX mounting medium (Sigma).

Digital Imaging and assessment of brain damage by cell counting

Digital immunofluorescence images were acquired using a Zeiss LSM 710 confocal laser-scanning microscope in conjunction with Zeiss ZEN 2010 software (vessel images). Overlays were constructed with freely-available ImageJ 1.44p software (National Institutes of Health, USA). Two independent assessors counted caspase-3 and Fluoro-Jade positive cells under blinded conditions, as previously described (12). For each animal, counts were obtained from the cortical region of a single coronal brain slice 1mm posterior to the bregma (200x magnification), which includes the left and right temporal and parietal lobes. The number of positive cells counted by each assessor was averaged, yielding a mean positive cell count/animal that was then used for statistical analyses.

Histological Analysis of Dendrite Morphology:

Brains were perfused with heparinized saline via transcardiac perfusion, isolated and processed/stained utilizing a commercially available Rapid GolgiStain kit (FD NeuroTechnologies Inc.; Columbia, USA). The kit uses a modified Golgi-Cox staining procedure originally described by Glaser and Van der Loos (24). Briefly, isolated brain tissue samples were immersed in a kit-provided solution containing mercuric chloride, potassium dichromate and potassium chromate in the dark for 8 days; this was followed by a 6-day incubation with tissue protection solution. The brain samples were then washed, embedded in 4% low gelling agarose, sectioned in the coronal plane (150 μm thickness; Campden Instruments 7000smz-2 vibrating microtome) and mounted onto gelatin-coated glass slides. The staining procedure was then completed using kit-provided developing/staining reagents, according to the manufacturer's instructions. Neurons and dendritic segments were imaged with stereology-based NIS Elements AR software on a Nikon Eclipse Ti2 microscope possessing motorized X-, Y-, and Z-focus for high-resolution image acquisition (Nikon Instruments Europe; Amsterdam, The Netherlands).

We analyzed both the basal and apical dendrite networks of pyramidal cortical neurons from the frontal cortex, using a quantitative approach originally described by Sholl (25). We utilized Image J software coupled with the semi-automated Simple Neurite Tracer plugin (both freely available from the NIH) to identify and digitally isolate the dendrite networks of a single cortical neuron from a 200x magnification hyperstack image. The center of the soma was marked with the pointer tool; dendrite morphology was then characterized by Sholl analysis (https://imagej.net/Sholl_Analysis, version 3.7.4), using 5 μm intervals to a maximal radius of 300 μm. This analysis characterizes dendrite morphology in terms of dendrite intersections (i.e., branching) and dendrite length. For each treatment group, 2-4 neurons per mouse from 4 mice were analyzed under blinded conditions.

To assess dendritic spine density (i.e., the number of small protrusions found on dendrites), we imaged 3rd branch order dendritic segments at 100x magnification. Spine density was measured as the number of spines per segment for the following segments: 20-50 μm from soma; 30-60 μm from soma; 50-80 μm from soma; and 60-100 μm from soma). This "sliding measurement" approach permits an assessment of how spine density changes over the length of dendritic branch. For each treatment group, spine density was measured in 2-4 pyramidal cortical neurons (2-4 third order branches per neuron) per mouse from 3-4 mice per group, under blinded conditions.

ONLINE FIGURE 1

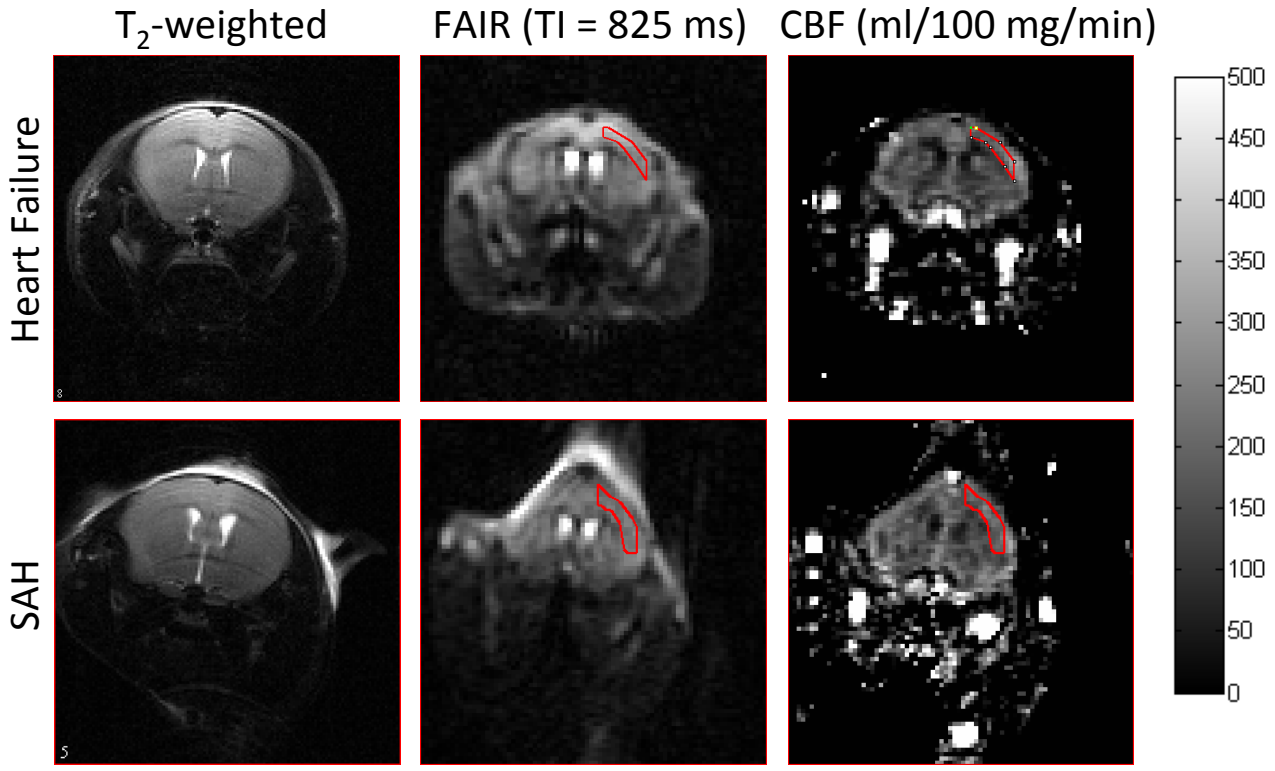

Region of interest placement in FAIR-EPI and analysis images.

Shown are representative anatomical T_2-weighted, flow-sensitive alternating inversion recovery (FAIR) T_1-weighted, and FAIR cerebral blood flow (CBF) maps for mice that underwent either the heart failure (top row) or subarachnoid hemorrhage (SAH; bottom row) surgical procedure. Regions of interest were manually drawn on forebrain slice FAIR images acquired at an inversion time (TI) of 825 ms using MIPAV software. The regions of interest encompass approximately 1 mm^3 of the cortical volume within 1 hemisphere, as shown. The regions of interest were then copied directly onto the CBF maps derived from FAIR images at the individual inversion times. SAH mice and sham-operated controls displayed varying degrees of echo-planar imaging (EPI) distortion (best visualized in the FAIR image); EPI-distortion was minimal in heart failure mice.

Abbreviations: CBF - cerebral blood flow; EPI - echo-planar imaging; FAIR - flow-sensitive alternating inversion recovery; SAH - subarachnoid hemorrhage.

ONLINE FIGURE 2

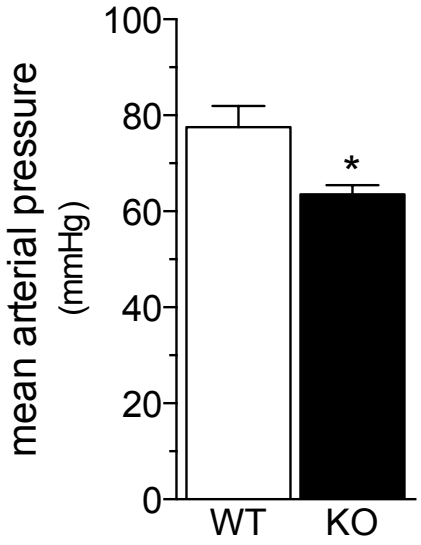

Mean arterial pressure in CFTR knockout mice

Mean arterial pressure is lower in cystic fibrosis transmembrane conductance regulator knockout mice (CFTR KO; $CFTR^{tm1Unc}$; n=6), relative to wild-type littermates (WT; n=6). * denotes $P<0.05$ for an unpaired t-test comparison.

Abbreviations: CFTR - cystic fibrosis transmembrane conductance regulator; KO - knockout; WT - wild-type

ONLINE FIGURE 3

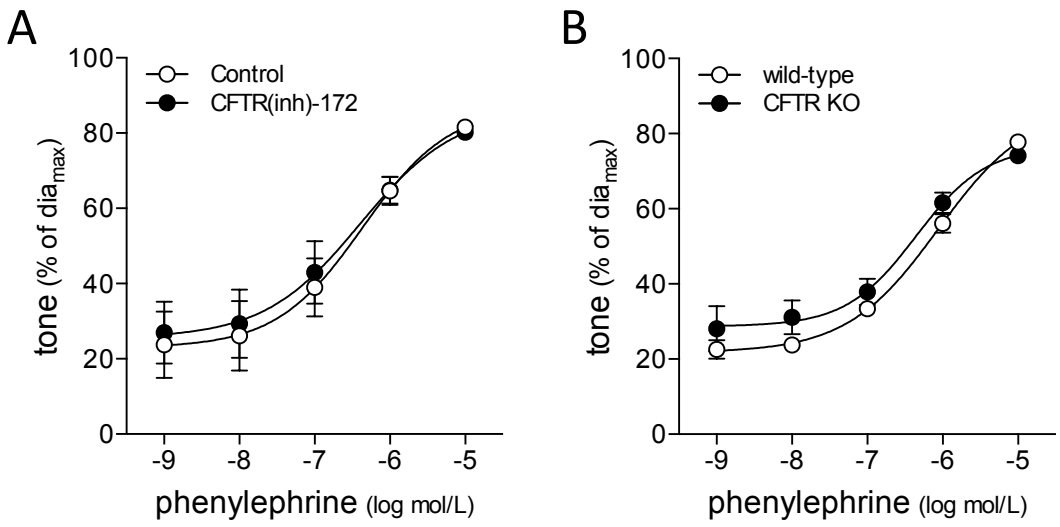

Phenylephrine responses in mouse cremaster arteries

Phenylephrine stimulates dose-dependent vasoconstriction in cremaster skeletal muscle arteries isolated from wild-type and cystic fibrosis transmembrane conductance regulator knockout mice (CFTR KO; CFTR^{tm1Unc}) mice. The phenylephrine dose-response relationship is not altered by **(A)** CFTR inhibition *in vitro* (100 nmol/L CFTR$_{(inh)}$-172 for 30 minutes) or **(B)** CFTR gene deletion.

Mean maximal vessel diameters at 60 mmHg (dia$_{max}$) are: wild-type (*Panel A*): 72±3 µm, n=5 from 4 mice; CFTR KO (*Panel B*): 88±4 µm, n=6 from 4 mice; and wild-type littermates (*Panel B*): 79±4 µm, n=5 from 2 mice. Dose-response curves in Panel A are compared with a paired two-way ANOVA (P=NS); curves in Panel B are compared with an unpaired two-way ANOVA (P=NS). For *Panel B*, KO and wild-type dia$_{max}$ values are not different (t-test P=NS).

Abbreviations: CFTR - cystic fibrosis transmembrane conductance regulator; dia$_{max}$ - maximal vessel diameter; KO - knockout; NS - not significant.

ONLINE FIGURE 4

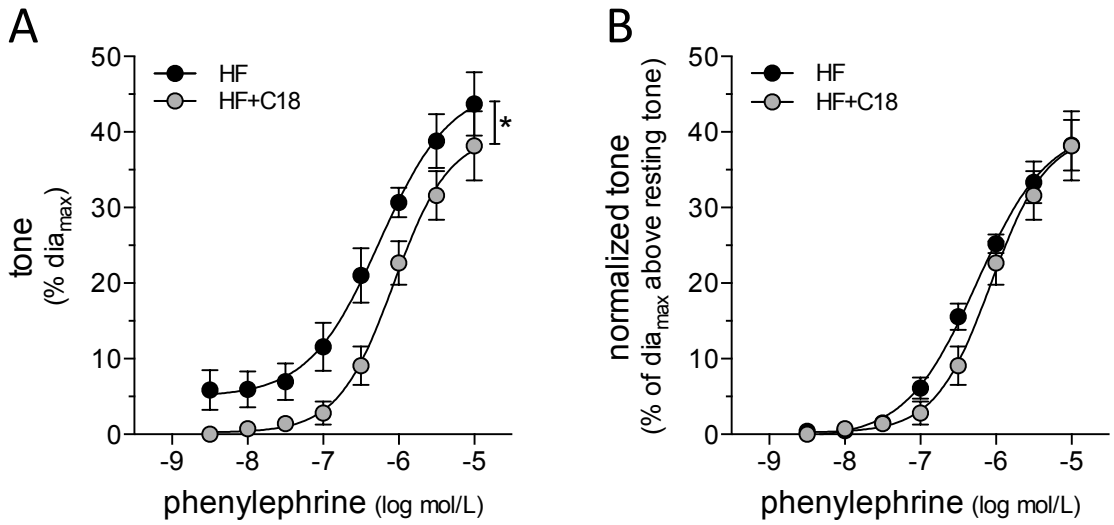

Phenylephrine responses in mouse posterior cerebral arteries following in vivo C18 treatment

(A) Phenylephrine stimulates dose-dependent vasoconstriction in posterior cerebral arteries isolated from mice with heart failure (HF) and mice with heart failure treated with C18 *in vivo* (3 mg/kg *i.p.* daily for 2 days). Statistical analysis identifies a significant difference between the two curves (i.e., there is significantly higher tone in arteries from HF, relative to HF+C18). However, **(B)** when the data are normalized to the basal tone ($tone_{active} - tone_{rest}$, where $tone_{active}$ is the tone at given phenylephrine concentration and $tone_{rest}$ is the tone immediately prior to stimulation), the dose-response relationships are not significantly different.

Mean maximal vessel diameters at 45 mmHg (dia_{max}) are: HF: 137±7 μm, n=5 from 3 mice and HF+C18: 140±8 μm, n=5 from 4 mice (t-test P=NS). In both panels, * denotes P<0.05 with a two-way ANOVA.

Abbreviations: dia_{max} - maximal vessel diameter; HF - heart failure; NS - not significant.

ONLINE FIGURE 5

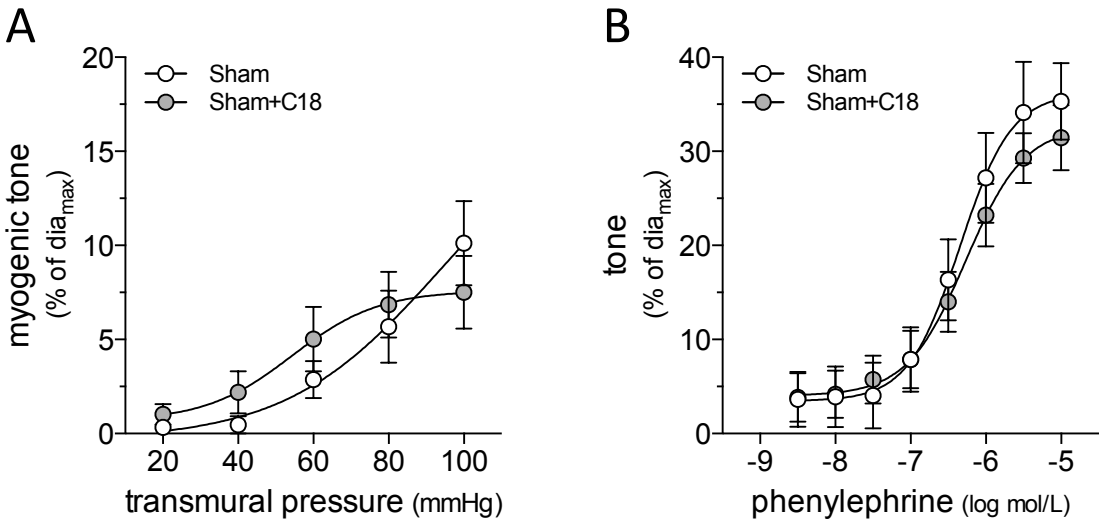

In vivo C18 treatment does not alter myogenic tone or phenylephrine responses in posterior cerebral arteries isolated from sham-operated mice

In vivo C18 treatment (3 mg/kg *i.p.* daily for 2 days) does not alter **(A)** myogenic tone or **(B)** phenylephrine responses in posterior cerebral arteries isolated from sham-operated mice.

Mean maximal vessel diameters at 45 mmHg (dia_{max}) in *Panel A*: Sham: 146±9 µm, n=5 from 3 mice and Sham+C18: 138±9 µm, n=7 from 4 mice (t-test P=NS); and in *Panel B*: Sham: 148±7 µm, n=6 from 3 mice and Sham+C18: 130±10 µm, n=5 from 3 mice (t-test P=NS). Curves in both panels are compared with a two-way ANOVA (P=NS).

Abbreviations: dia_{max} - maximal vessel diameter; NS - not significant.

ONLINE FIGURE 6

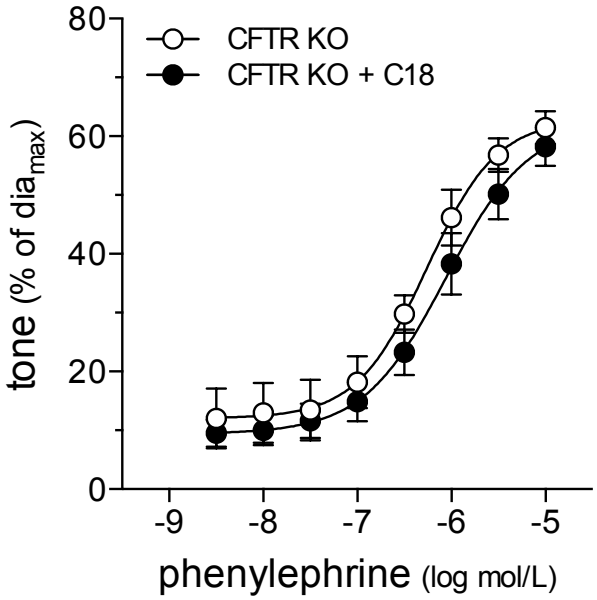

Phenylephrine responses in posterior cerebral arteries from CFTR knockout mice treated with C18

Phenylephrine stimulates dose-dependent vasoconstriction in posterior cerebral arteries isolated from cystic fibrosis transmembrane conductance regulator knockout mice (CFTR KO; CFTR^{tm1Unc}). *In vivo* C18 treatment (3 mg/kg *i.p.* daily for 2 days) does not alter the phenylephrine dose-response relationship.

Mean maximal vessel diameters at 45 mmHg (dia$_{max}$) are: CFTR KO: 142±5 µm, n=6 from 3 mice and CFTR KO + C18: 145±5 µm, n=6 from 3 mice (t-test P=NS). Curves are compared with a two-way ANOVA (P=NS).

Abbreviations: CFTR - cystic fibrosis transmembrane conductance regulator; dia$_{max}$ - maximal vessel diameter; KO - knockout; NS - not significant.

ONLINE FIGURE 7

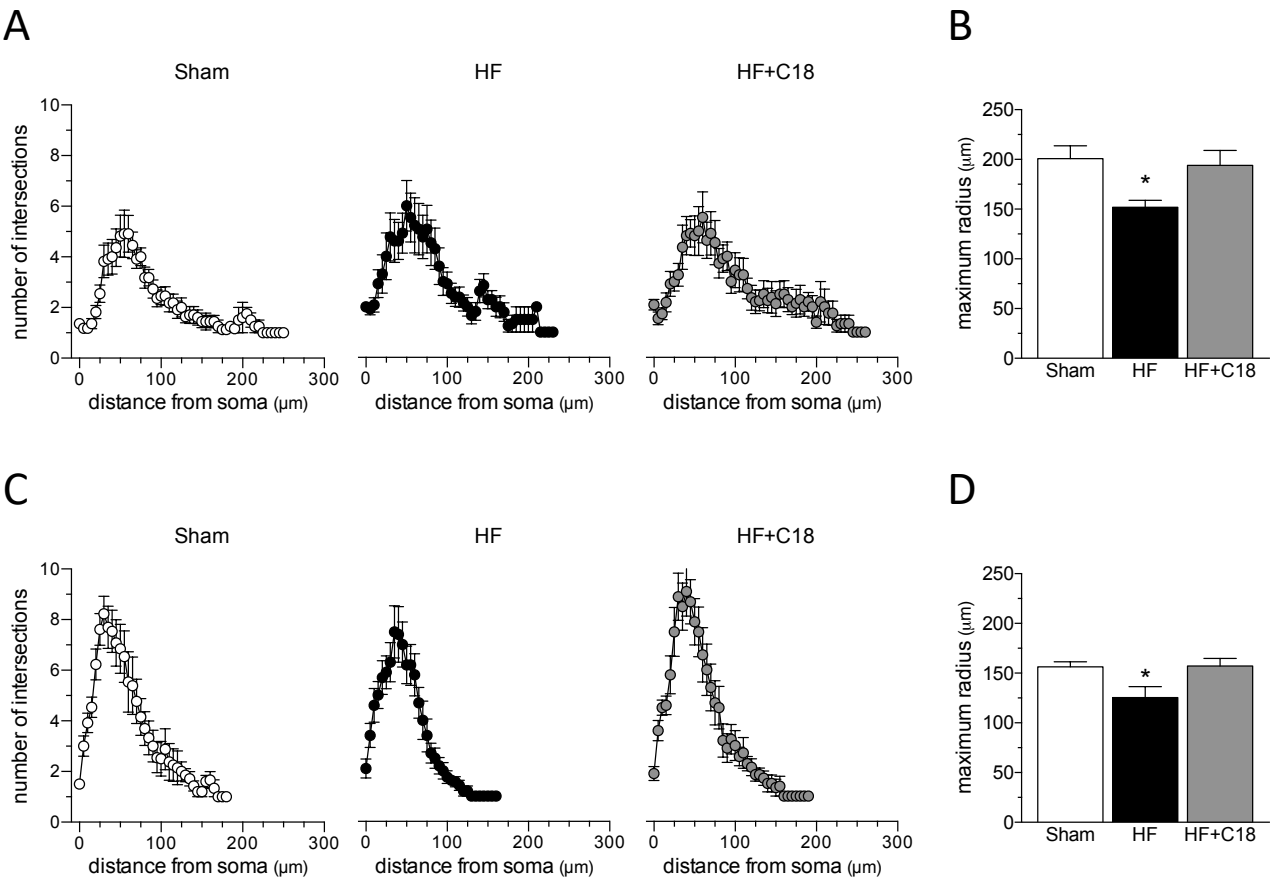

Breakdown Sholl analysis of apical and basal dendrites

(A) Shown are Sholl analysis histograms plotting the number of dendrite intersections (i.e., dendritic branching) versus dendritic length (i.e., distance from neuronal soma) for ***apical dendrites***. No differences in branching morphology are observed across the sham (n=13 neurons from N=4 mice), heart failure (HF; n=11; N=4) and HF+C18 (3 mg/kg *i.p.* daily for 2 weeks; n=11; N=4) groups; however, apical dendritic length is shorter in HF mice, relative to the sham and HF+C18 groups. Accordingly, **(B)** mean apical dendrite length (i.e., maximum radius) is significantly reduced in HF mice relative to sham mice; this effect is normalized by C18 treatment. Similarly, **(C)** Sholl analysis histograms for ***basal dendrites*** show no differences in branching morphology across the sham (n=12; N=4), HF (n=13; N=4) and HF+C18 (n=11; N=4) groups; however, basal dendritic length is shorter in HF mice, relative to the sham and HF+C18 groups. Accordingly, **(D)** mean basal dendrite length (i.e., maximum radius) is significantly reduced in HF mice relative to sham mice, an effect that is normalized by C18 treatment. * denotes $P<0.05$ for unpaired comparisons to the sham with a one-way ANOVA and Dunnett's *post-hoc* test.

Abbreviations: HF - heart failure.

ONLINE FIGURE 8

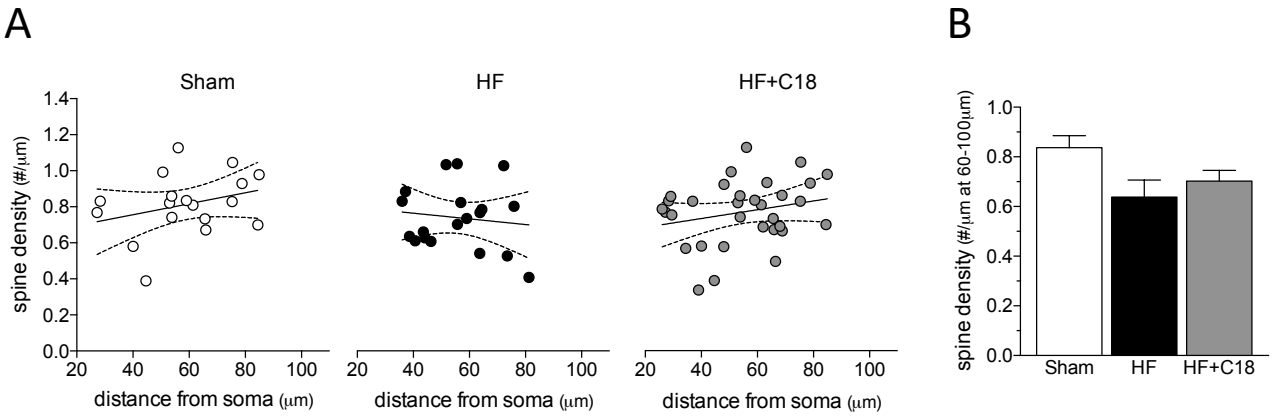

Spine density analysis of apical dendrites

(A) In sham (n=8 neurons from N=4 mice), heart failure (HF; n=6; N=3) and HF+C18 mice (3 mg/kg *i.p.* daily for 2 weeks; n=10; N=4), ***apical dendrite*** spine density (i.e., a measure of synapse density) is relatively consistent over the length of the dendrite, yielding slopes that are not statistically different from zero. **(B)** Although tendencies are present, mean apical dendrite spine density measures at 60-100μm from soma does not reach statistical significance. The groups were statistically compared with a one-way ANOVA (P=NS).

Abbreviations: HF - heart failure; NS - not significant.

ONLINE FIGURE 9

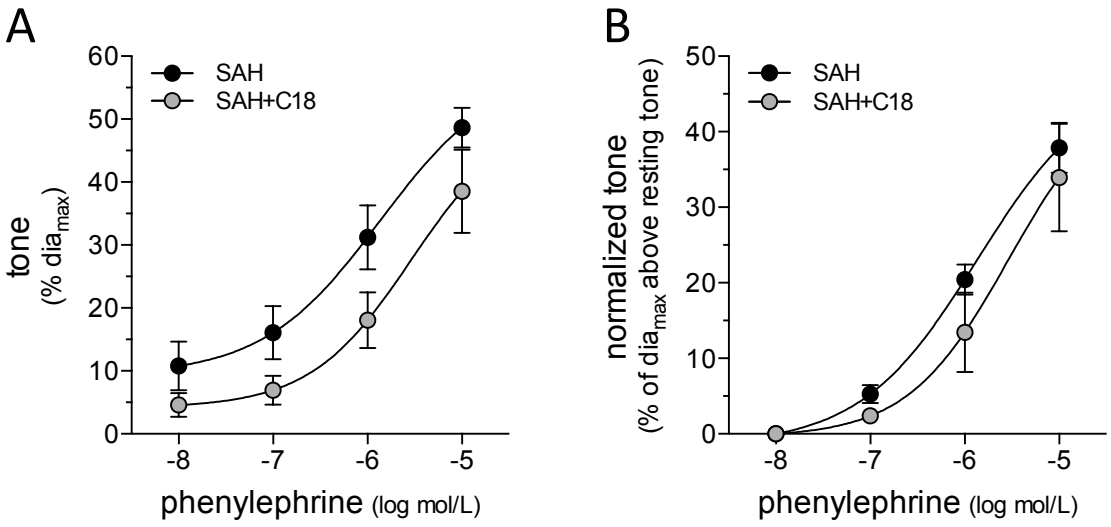

Phenylephrine responses in mouse olfactory cerebral arteries following in vivo C18 treatment

(A) Phenylephrine stimulates dose-dependent vasoconstriction in olfactory cerebral arteries isolated from mice with subarachnoid hemorrhage (SAH) and SAH mice treated with C18 *in vivo* (3 mg/kg *i.p.* daily for 2 days). Although there is a clear tendency for separation, the two curves are not statistically different. **(B)** When the data are normalized to the basal tone ($tone_{active} - tone_{rest}$, where $tone_{active}$ is the tone at given phenylephrine concentration and $tone_{rest}$ is the tone immediately prior to stimulation), the separation of the dose-response relationships is minimal.

Mean maximal vessel diameters at 45 mmHg (dia_{max}) are: SAH: 109±6 µm, n=6 from 6 mice and SAH+C18: 105±12 µm, n=5 from 4 mice (t-test P=NS). Curves are compared with a two-way ANOVA.

Abbreviations: dia_{max} - maximal vessel diameter; NS - not significant; SAH - subarachnoid hemorrhage.

ONLINE FIGURE 10

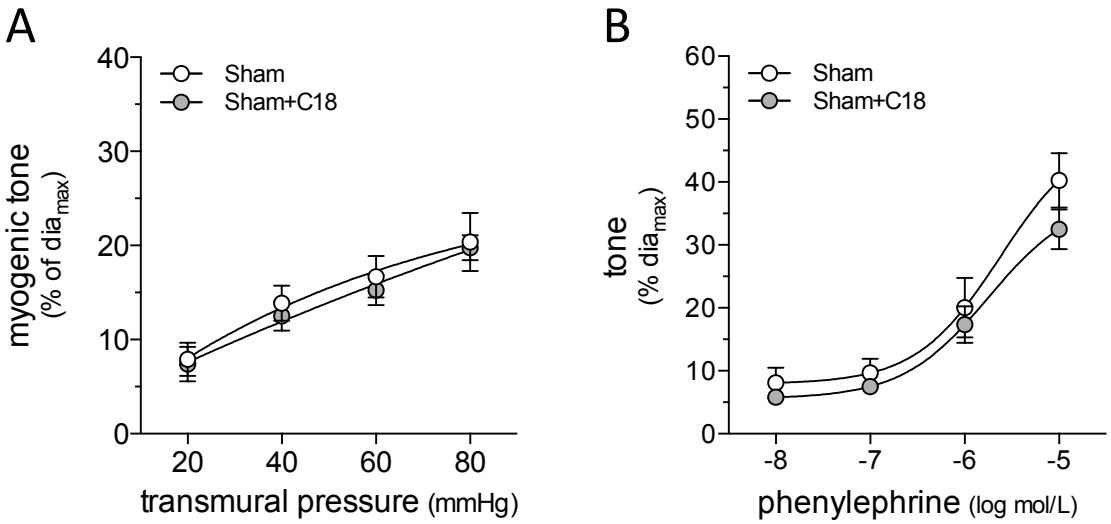

C18 does not impact myogenic tone or phenylephrine responses in sham-operated mice

In vivo C18 treatment (3 mg/kg *i.p.* daily for 2 days) does not alter **(A)** myogenic tone or **(B)** the phenylephrine dose-response relationship in olfactory cerebral arteries isolated from sham-operated mice.

Mean maximal vessel diameters at 45 mmHg (dia_{max}) are: Sham: 113±3 µm, n=5 from 3 mice; and Sham+C18: 110±8 µm, n=6 from 4 mice (t-test P=NS). Curves are compared with a two-way ANOVA.

Abbreviations: dia_{max} - maximal vessel diameter; NS - not significant.

ONLINE FIGURE 11

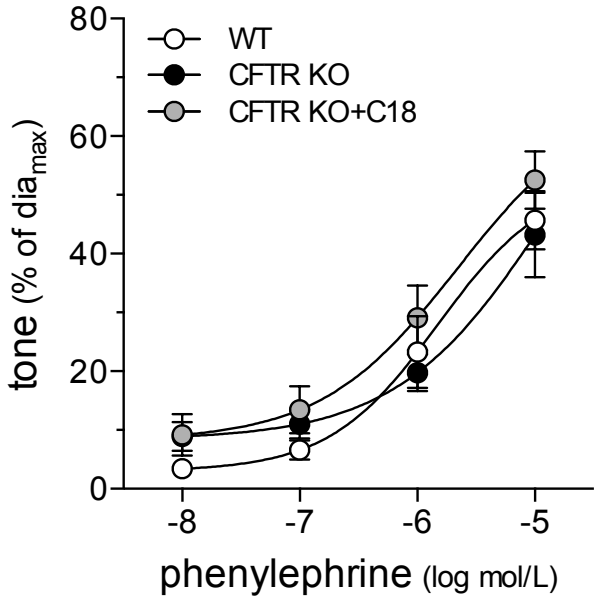

Phenylephrine responses in olfactory cerebral arteries isolated from CFTR knockout mice

Phenylephrine stimulates dose-dependent vasoconstriction in olfactory cerebral arteries isolated from cystic fibrosis transmembrane conductance regulator knockout mice (CFTR KO; CFTR^{tm1Unc}) that is similar to that of wild-type (WT) littermates. *In vivo* C18 treatment (3 mg/kg *i.p.* daily for 2 days) does not alter the phenylephrine dose-response relationship.

Mean maximal vessel diameters at 45 mmHg (dia$_{max}$) are: WT: 98±6 µm, n=8 from 4 mice; CFTR KO: 110±8 µm, n=5 from 4 mice and CFTR KO + C18: 96±6 µm, n=6 from 3 mice (one-way ANOVA P=NS). Curves are compared with a two-way ANOVA.

Abbreviations: CFTR - cystic fibrosis transmembrane conductance regulator; dia$_{max}$ - maximal vessel diameter; KO - knockout; NS - not significant; WT - wild-type.

ONLINE FIGURE 12

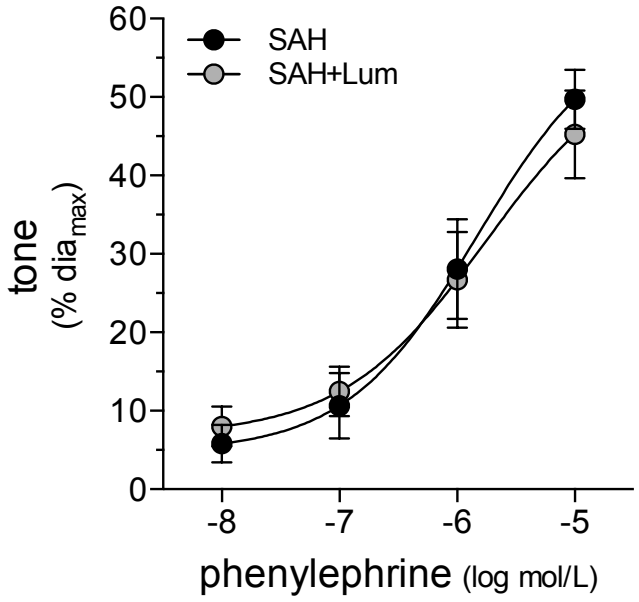

Phenylephrine responses in mouse olfactory cerebral arteries following in vivo lumacaftor treatment

In vivo lumacaftor (Lum) treatment (3 mg/kg *i.p.* daily for 2 days) does not alter the phenylephrine dose-response relationship in olfactory cerebral arteries isolated from mice with subarachnoid hemorrhage (SAH).

Mean maximal vessel diameters at 45 mmHg (dia_{max}) are: SAH: 86±2 µm, n=6 from 3 mice; and SAH+Lum: 87±4 µm, n=7 from 4 mice (t-test P=NS). Curves are compared with a two-way ANOVA.

Abbreviations: dia_{max} - maximal vessel diameter; Lum - lumacaftor; NS - not significant; SAH - subarachnoid hemorrhage.

ONLINE TABLE 1

Mouse characteristics and hemodynamic parameters in wild-type and CFTR$^{\Delta F508}$ mutant mice

	Wild Type	CFTR$^{\Delta F508}$	n
Body weight (g)	30 ± 2	**25 ± 1 ***	5
Heart rate (min^{-1})	499 ± 19	514 ± 10	5
LVEF (%)	68 ± 1	66 ± 2	5
Stroke volume (µl)	43 ± 2	**36 ± 1 ***	5
SBP (mmHg)	107 ± 4	96 ± 4	5
DBP (mmHg)	75 ± 4	66 ± 2	5
MAP (mmHg)	86 ± 4	76 ± 3	5
CO (ml/min)	22 ± 2	18 ± 1	5
TPR (mmHg/ml)	4.0 ± 0.3	4.2 ± 0.3	5

Data are mean ± SEM. * denotes *P*<0.05 for an unpaired comparison (t-test)

Acronyms: LVEF – Left ventricular ejection fraction; SBP – systolic blood pressure; DBP − diastolic blood pressure; MAP – mean arterial pressure; CO – cardiac output; TPR − total peripheral resistance.

ONLINE TABLE 2

Mouse characteristics and hemodynamic parameters

	Sham		HF		HF+C18	
	Mean ± SEM	**n**	**Mean ± SEM**	**n**	**Mean ± SEM**	**n**
Body weight (g)	24.1 ± 2.3	6	25.1 ± 1.4	8	24.5 ± 0.9	9
Heart weight (g)	0.138 ± 0.017	6	**0.180 ± 0.007 ***	8	**0.192 ± 0.009 ***	9
Heart/Body(mg/g)	5.67 ± 0.26	6	**7.23 ± 0.20 ***	8	**7.86 ± 0.25 ***	9
Lung weight (g)	0.134 ± 0.010	6	**0.165 ± 0.006 ***	8	**0.169 ± 0.007 ***	9
Liver weight (g)	1.08 ± 0.14	6	1.08 ± 0.08	8	1.12 ± 0.08	9
Heart rate (min^{-1})	520 ± 10	6	465 ± 15	8	462 ± 35	8
LVEF (%)	89.8 ± 1.2	6	**56.9 ± 1.5 ***	8	**56.5 ± 1.2 ***	8
Stroke volume (µl)	19.5 ± 0.8	6	**13.0 ± 1.1 ***	8	**14.2 ± 1.1***	8
MAP (mmHg)	66 ± 1	6	**58 ± 1 ***	6	60 ± 3	6
CO (ml/min)	10.1 ± 0.4	6	**6.0 ± 0.5 ***	8	**6.4 ± 0.5 ***	8
TPR (mmHg/ml)	6.59 ± 0.29	6	**9.08 ± 0.60 ***	6	**9.07 ± 0.90 ***	6
CBF (ml/100g*min)	176 ± 9	6	**134 ± 4 ***	8	161 ± 8	8

*** denotes *P*<0.05 for an unpaired comparison to the sham (one-way ANOVA with Dunnett's test)**

Acronyms: LVEF − Left ventricular ejection fraction; MAP − mean arterial pressure; CO − cardiac output; TPR − total peripheral resistance; CBF − cerebral blood flow; HF – Heart failure.

ONLINE TABLE 3

Sholl analysis of pyramidal cortical neurons from the frontal cortex

	Complete Neuron					
	Sham		HF		HF+C18	
	Mean ± SEM	n	Mean ± SEM	n	Mean ± SEM	n
Maximum Radius (µm)	206.7 ± 12.5	12	**161.3 ± 6.8** *	12	205.5 ± 11.3	11
Mean Intersections	5.4 ± 0.5	13	6.2 ± 0.8	13	6.5 ± 0.3	11
Maximum Intersections	13.9 ± 1.5	13	13.9 ± 1.5	13	15.3 ± 0.9	11
Maximum Intersection Radius (µm)	39.2 ± 4.7	13	46.9 ± 4.6	13	47.3 ± 4.3	11
Critical r Value (dendrite maximum)	12.2 ± 1.2	13	12.7 ± 1.4	13	14.0 ± 1.0	11
Ramification Index	4.1 ± 0.6	13	2.6 ± 0.3	12	2.8 ± 0.3	11
Critical Radius (µm)	41.6 ± 3.2	13	46.3 ± 3.7	13	47.8 ± 3.0	11

	Apical Dendrites					
	Sham		HF		HF+C18	
	Mean ± SEM	n	Mean ± SEM	n	Mean ± SEM	n
Maximum Radius (µm)	200.8 ± 13.0	13	**151.8 ± 7.1** *	11	194.1 ± 15.0	11
Mean Intersections	2.4 ± 0.2	13	3.5 ± 0.5	13	3.1 ± 0.2	11
Maximum Intersections	5.8 ± 0.7	13	7.7 ± 1.1	13	7.5 ± 0.8	11
Maximum Intersection Radius (µm)	44.2 ± 5.1	13	61.9 ± 11.3	13	60.9 ± 7.5	11
Critical r Value (dendrite maximum)	5.0 ± 0.6	13	6.5 ± 1.1	13	5.9 ± 0.7	11
Ramification Index	4.2 ± 0.4	13	3.5 ± 0.3	13	4.7 ± 0.8	11
Critical Radius (µm)	63.3 ± 8.0	13	62.5 ± 9.4	13	58.8 ± 7.6	11

	Basal Dendrites					
	Sham		HF		HF+C18	
	Mean ± SEM	n	Mean ± SEM	n	Mean ± SEM	n
Maximum Radius (µm)	156.4 ± 5.1	11	**125.4 ± 11.0** *	13	157.3 ± 7.5	11
Mean Intersections	5.0 ± 0.6	11	4.5 ± 0.6	13	4.8 ± 0.3	11
Maximum Intersections	9.9 ± 0.7	11	9.1 ± 0.9	13	10.6 ± 0.7	11
Maximum Intersection Radius (µm)	34.6 ± 4.0	11	27.3 ± 3.2	11	40.0 ± 2.9	11
Critical r Value (dendrite maximum)	9.3 ± 0.7	11	8.4 ± 0.9	13	9.6 ± 0.7	11
Ramification Index	4.1 ± 0.8	12	3.2 ± 0.6	13	2.6 ± 0.4	11
Critical Radius (µm)	37.2 ± 3.4	11	37.8 ± 3.0	13	41.5 ± 3.2	11

*** denotes *P*<0.05 for an unpaired comparison to the sham (one-way ANOVA with Dunnett's test)**

ONLINE TABLE 4

Quantitative PCR Primer Sequences

Species	Gene	Primer Sequences (5' to 3')	Product Size (bp)	Efficiency	Accession no.
Mouse	**CFTR**	CTGGACCACACCAATTTTGAGG GCGTGGATAAGCTGGGGAT	162	1.05	NM_021050
Mouse	**HMBS**	CCCGTAACATTCCAAGAGGA CCTGTGCCCTACAGACCAGT	147	1.08	NM_013551
Mouse	**G6PD**	CACAGTGGACGACATCCGAAA AGCTACATAGGAATTACGGGCAA	103	1.02	NM_008062
Human	**CFTR**	AGCATTTGCTGATTGCACAG ACTGCCGCACTTTGTTCTCT	101	0.99	NM_000492
Hamster	**GAPDH**	CAATGACCCCTTCATTGACC GACAAGCTTCCCGTTCTCAG	106	0.95	DQ403055

CFTR - cystic fibrosis transmembrane conductance regulator; HMBS - hydroxymethylbilane synthase; G6PD - glucose-6-phosphate dehydrogenase; GAPDH - glyceraldehyde 3-phosphate dehydrogenase.

ONLINE INFORMATION REFERENCES

1. Cui L, Aleksandrov L, Chang XB, et al. Domain interdependence in the biosynthetic assembly of CFTR. J Mol Biol 2007;365:981-94.
2. van Doorninck JH, French PJ, Verbeek E, et al. A mouse model for the cystic fibrosis delta F508 mutation. EMBO J 1995;14:4403-11.
3. Van Goor F, Straley KS, Cao D, et al. Rescue of DeltaF508-CFTR trafficking and gating in human cystic fibrosis airway primary cultures by small molecules. Am J Physiol Lung Cell Mol Physiol 2006;290:L1117-30.
4. French PJ, van Doorninck JH, Peters RH, et al. A delta F508 mutation in mouse cystic fibrosis transmembrane conductance regulator results in a temperature-sensitive processing defect in vivo. J Clin Invest 1996;98:1304-12.
5. Zeiher BG, Eichwald E, Zabner J, et al. A mouse model for the delta F508 allele of cystic fibrosis. J Clin Invest 1995;96:2051-64.
6. Wilke M, Buijs-Offerman RM, Aarbiou J, et al. Mouse models of cystic fibrosis: phenotypic analysis and research applications. J Cyst Fibros 2011;10 Suppl 2:S152-71.
7. Lavelle GM, White MM, Browne N, McElvaney NG, Reeves EP. Animal Models of Cystic Fibrosis Pathology: Phenotypic Parallels and Divergences. Biomed Res Int 2016;2016:5258727.
8. Nilius B, Droogmans G. Amazing chloride channels: an overview. Acta Physiol Scand 2003;177:119-47.
9. Hoefer J, Azam MA, Kroetsch JT, et al. Sphingosine-1-phosphate-dependent activation of p38 MAPK maintains elevated peripheral resistance in heart failure through increased myogenic vasoconstriction. Circ Res 2010;107:923-33.
10. Meissner A, Yang J, Kroetsch JT, et al. Tumor Necrosis Factor-α-Mediated Downregulation of the Cystic Fibrosis Transmembrane Conductance Regulator Drives Pathological Sphingosine-1-Phosphate Signaling in a Mouse Model of Heart Failure. Circulation 2012;125:2739-50.
11. Yang J, Hossein Noyan-Ashraf M, Meissner A, et al. Proximal Cerebral Arteries Develop Myogenic Responsiveness in Heart Failure via Tumor Necrosis Factor-α-Dependent Activation of Sphingosine-1-Phosphate Signaling. Circulation 2012;126:196-206.
12. Yagi K, Lidington D, Wan H, et al. Therapeutically Targeting Tumor Necrosis Factor-α/Sphingosine-1-Phosphate Signaling Corrects Myogenic Reactivity in Subarachnoid Hemorrhage. Stroke 2015;46:2260-70.
13. Kim SG. Quantification of relative cerebral blood flow change by flow-sensitive alternating inversion recovery (FAIR) technique: application to functional mapping. Magn Reson Med 1995;34:293-301.
14. Herscovitch P, Raichle ME. What is the correct value for the brain--blood partition coefficient for water? J Cereb Blood Flow Metab 1985;5:65-9.
15. Foley LM, Hitchens TK, Kochanek PM, Melick JA, Jackson EK, Ho C. Murine orthostatic response during prolonged vertical studies: effect on cerebral blood flow measured by arterial spin-labeled MRI. Magn Reson Med 2005;54:798-806.
16. Foltz WD, Porter DA, Simeonov A, et al. Readout-segmented echo-planar diffusion-weighted imaging improves geometric performance for image-guided radiation therapy of pelvic tumors. Radiother Oncol 2015;117:525-31.

17. Sharma M, Benharouga M, Hu W, Lukacs GL. Conformational and temperature-sensitive stability defects of the delta F508 cystic fibrosis transmembrane conductance regulator in post-endoplasmic reticulum compartments. J Biol Chem 2001;276:8942-50.
18. Malik FA, Meissner A, Semenkov I, et al. Sphingosine-1-Phosphate Is a Novel Regulator of Cystic Fibrosis Transmembrane Conductance Regulator (CFTR) Activity. PLoS One 2015;10:e0130313.
19. Lin CL, Calisaneller T, Ukita N, Dumont AS, Kassell NF, Lee KS. A murine model of subarachnoid hemorrhage-induced cerebral vasospasm. J Neurosci Methods 2003;123:89-97.
20. Parra A, McGirt MJ, Sheng H, Laskowitz DT, Pearlstein RD, Warner DS. Mouse model of subarachnoid hemorrhage associated cerebral vasospasm: methodological analysis. Neurol Res 2002;24:510-6.
21. Aum DJ, Vellimana AK, Singh I, et al. A novel fluorescent imaging technique for assessment of cerebral vasospasm after experimental subarachnoid hemorrhage. Sci Rep 2017;7:9126.
22. Brilstra EH, Rinkel GJ, Algra A, van Gijn J. Rebleeding, secondary ischemia, and timing of operation in patients with subarachnoid hemorrhage. Neurology 2000;55:1656-60.
23. Macdonald RL. Delayed neurological deterioration after subarachnoid haemorrhage. Nat Rev Neurol 2014;10:44-58.
24. Glaser EM, Van der Loos H. Analysis of thick brain sections by obverse-reverse computer microscopy: application of a new, high clarity Golgi-Nissl stain. J Neurosci Methods 1981;4:117-25.
25. Sholl DA. Dendritic organization in the neurons of the visual and motor cortices of the cat. J Anat 1953;87:387-406.